IOPscience iopscience.iop.org

Home Search Collections Journals About Contact us My IOPscience

Thermo-stability of acrylate based holographic polymer dispersed liquid crystal gratings

This article has been downloaded from IOPscience. Please scroll down to see the full text article.

2009 J. Phys. D: Appl. Phys. 42 115504

(http://iopscience.iop.org/0022-3727/42/11/115504)

View the table of contents for this issue, or go to the journal homepage for more

Download details:
IP Address: 159.226.165.151
The article was downloaded on 05/09/2012 at 06:10

Please note that terms and conditions apply.

J. Phys. D: Appl. Phys. **42** (2009) 115504 (12pp) doi:10.1088/0022-3727/42/11/115504

Thermo-stability of acrylate based holographic polymer dispersed liquid crystal gratings

Zhigang Zheng[1,2], Lishuang Yao[3], Ran Zhang[1], Zhongfei Zou[1], Yan Liu[1], Yonggang Liu[1] and Li Xuan[1]

[1] State Key Laboratory of Applied Optics, Changchun Institute of Optics, Fine Mechanics and Physics Chinese Academy of Sciences, Changchun 130033, People's Republic of China
[2] Department of Physics, East China University of Science and Technology, 130 Meilong Road, Shanghai 200237, People's Republic of China
[3] Centre of Display Research, Hong Kong University of Science and Technology, Clear Water Bay, Kowloon, Hong Kong

E-mail: zhigang1982@sina.com

Received 6 October 2008, in final form 31 March 2009
Published 14 May 2009
Online at stacks.iop.org/JPhysD/42/115504

Abstract
The thermo-stability of acrylate based holographic polymer dispersed liquid crystal gratings has been evaluated with regard to their morphology, diffraction efficiency, Bragg angle and electro-optical tunable performance. Our studies indicate that the thermo-stability is closely related to the chemical structure of the monomers in the grating. Usually, a more rigid molecular structure forms a more stable morphology. Another important aspect, the reaction efficiency of the system, shows that a highly efficient photoreaction leads to a dense polymer network and high ene-conversion, thus promoting the phase separation of the liquid crystal and enhancing the thermo-stability. We also find that a higher average functionality of the monomers can improve grating thermo-stability due to denser crosslinked polymers and more complete phase separation.

(Some figures in this article are in colour only in the electronic version)

Abbreviations

H-PDLC	holographic polymer dispersed liquid crystal
DN	monomer mixture composed of DPHPA and NPGDA
DP	monomer mixture composed of DPHPA and PDDA
DB	monomer mixture composed of DPHPA and BPFEDA
DP(2.88)	monomer mixture with an average functionality of 2.88
H-PDLC(n)	the grating fabricated from the mixture: DN+LC
H-PDLC(p)	the grating fabricated from the mixture: DP+LC
H-PDLC(b)	the grating fabricated from the mixture: DB+LC
H-PDLC(2.88)	the grating fabricated from the mixture: DP(2.88)+LC
P_{DN}	polymer formed from the DN mixture
P_{DP}	polymer formed from the DP mixture
P_{DB}	polymer formed from the DB mixture

1. Introduction

As a novel functional material, polymer dispersed liquid crystal (PDLC) has attracted much interest because of its excellent optical and electro-optical modulation properties. Previous studies show that PDLC materials can be used to fabricate photonic elements in two ways: by photomask technology [1–6], and by holography [7–12]. The former is restricted by etching technique limitations and is more complicated.

 © 2009 IOP Publishing Ltd Printed in the UK

Holography is simpler, time saving and low cost, so it is preferred in practice.

When a liquid crystal (LC)/monomer mixture is irradiated by an intensity modulated interference field, the monomer crosslinks in the high intensity zone, forming a solid elastic network, and LC is squeezed out of the network to form nano-scaled droplets. A periodic chemical potential gradient is thus constructed, and subsequently, the monomer and LC start to diffuse in opposite directions due to this gradient [13, 14]. Because of the diffusion, the monomers can polymerize continually and the LC droplets coalesce together, resulting in polymerization-induced phase separation (PIPS) [15–17] and finally forming a well-defined structure with alternating polymer-rich and LC-rich lamellas. This is the so-called holographic PDLC (H-PDLC) grating [17] which can be widely used in optical communication, integrated optics, optical data storage, etc [18–20]. Current research is mostly focused on ways to improve the morphology, enhance the optical efficiency, and decrease the threshold voltage of the grating [21–25]. Some groups use dynamic modelling to study the grating formation and phase separation [26–30]. For some special applications of this grating, such as in thermal and electric sensors [31], transmission mode spectrometers [32], optical shifters and attenuators [33, 34], distributed feedback lasers [35] and colour display fields [36, 37], the thermo-stability is another important aspect which, however, has been rarely noted. Some earlier studies on the stability of PDLC devices showed that device stability can be enhanced by improving the material properties [38–40]. Recently, Crawford's and Kim's groups have observed the shrinkage of acrylate based H-PDLC gratings under irradiation or heating [41–43]. However, all the above studies were only experimentally or phenomenological; other factors which could influence the stability of H-PDLC gratings were not discussed. The reasons for the instability, the decisive aspects of thermo-stability, and how to improve this in practice are all unclear, so further studies are still necessary.

To solve these problems, we used three kinds of materials to fabricate H-PDLC gratings and evaluated their thermo-stabilities from the diffraction efficiency, Bragg angle, electro-optical properties and morphology. A scanning electron microscope (SEM) and atomic force microscope (AFM) were used to observe the morphology stability. Thermogravimetry (TG) was used to analyse the stability of the polymer materials in the grating. The photoreaction kinetics during exposure was detected by Fourier transform infrared (FTIR) spectroscopy. Based on these characterization methodologies, the thermo-stability is discussed from three aspects, and some feasible ways to improve it are suggested.

The materials and the characterization methods used in our experiments are presented in the following section. The experimental results are given in section 3. In section 4, some necessary analyses about thermo-stability are discussed. Conclusions of the study are given in the last section.

2. Materials and measurements

2.1. Materials preparation

The monomers used in the experiments were mainly pentafunctional dipentaerythritol hydroxyl pentaacrylate (DPHPA, $n = 1.49$ at 20 °C, from Aldrich), and three kinds of difunctional acrylate: neopentyl glycol diacrylate (NPGDA, $n = 1.544$ at 20 °C, provided by Eastern Acrylic Chem. Tech. Co., Ltd., Beijing), phthalic diglycol diacrylate (PDDA, $n = 1.545$ at 20 °C, also from Eastern Acrylic) and bisphenol F ethoxylate diacrylate (BPFEDA, $n = 1.541$ at 20 °C, from Aldrich). The purities of all the monomers were higher than 97%. To investigate the effects of molecular structure on thermo-stability, three kinds of monomer mixtures were prepared and their average functionalities controlled around 3.39. In addition, a small amount of photoinitiator Rose Bengal (RB, 0.5 wt% of the total weight of mixture) and coinitiator n-phenylglycine (NPG, 2 wt% of the total weight of mixture) were also added for the monomer photoreaction at a wavelength of 532 nm. The compositions of the three mixtures are given in table 1. These mixtures were stirred at 65 °C for about 12 h. Then, some nematic LC TEB30A ($\Delta n = 0.1703$, $n_e = 1.6925$, $T_{NI} = 61.2$ °C, from Slichem Co., Ltd., Shi Jia Chuang, China) were added into the mixture in a weight ratio of 3 : 7 (LC/monomers) and re-stirred at 65 °C for another 12 h. To clarify the influence of the monomers' average functionality on thermo-stability of the H-PDLC grating, a little N-vinyl-2-pyrrolidinone (NVP) was used to modulate the functionality to 2.88 for sample DP(2.88), as shown in table 1. The ratio of the LC/monomers was still 3 : 7. Figure 1 shows the chemical structures of the monomers.

2.2. Grating fabrication and measurements

The LC/monomer mixtures were injected into the ITO cells by capillary action. The cell gap was maintained by 12 μm thick transparent spacers. Next, the cells were laid statically in a dark box for several minutes to avoid convection of the mixture in the cells and to ensure that the system was relatively static before exposure. These cells were then exposed for about 15 min to two coherent laser beams (of wavelength 532 nm) with an intensity of 3.6 mW cm^{-2}. To distinguish between the H-PDLC gratings fabricated by different mixtures, the samples were labelled H-PDLC(n), H-PDLC(p), H-PDLC(b) and H-PDLC(2.88), corresponding to the gratings fabricated from DN, DP, DB and DP(2.88) monomer mixtures, respectively. All samples were kept in a dark box for 10 days prior to measurements.

Before thermo-stability testing, the gratings were baked in a high temperature oven in steps of 25 °C from room temperature to 250 °C for about 10 min. They were then cooled to room temperature and tested. The diffraction efficiencies and electro-optical tunable characteristics were measured at 633 nm with a 50 Hz sinusoidal wave signal. The Bragg angle was measured by a homemade precision rotation station.

An AFM (Nanoscope Dimension 3100, USA) and SEM (Hitachi S-4800, Japan) were used for morphological

Table 1. Composition of monomer mixtures used in the experiments.

Sample[a]	DPHPA (g)	NPGDA (g)	PDDA (g)	BPFEDA (g)	NVP (mg)	NPG (mg)	RB (mg)
DN	0.67	0.32				29.5	7.4
DP	0.67		0.67			40.0	10.0
DB	0.67			0.72		41.4	10.4
DP(2.88)	0.55		0.55		69.1	34.0	8.0

[a] The average functionality is 3.39 for the mixtures DN, DP and DB and 2.88 for DP (2.88).

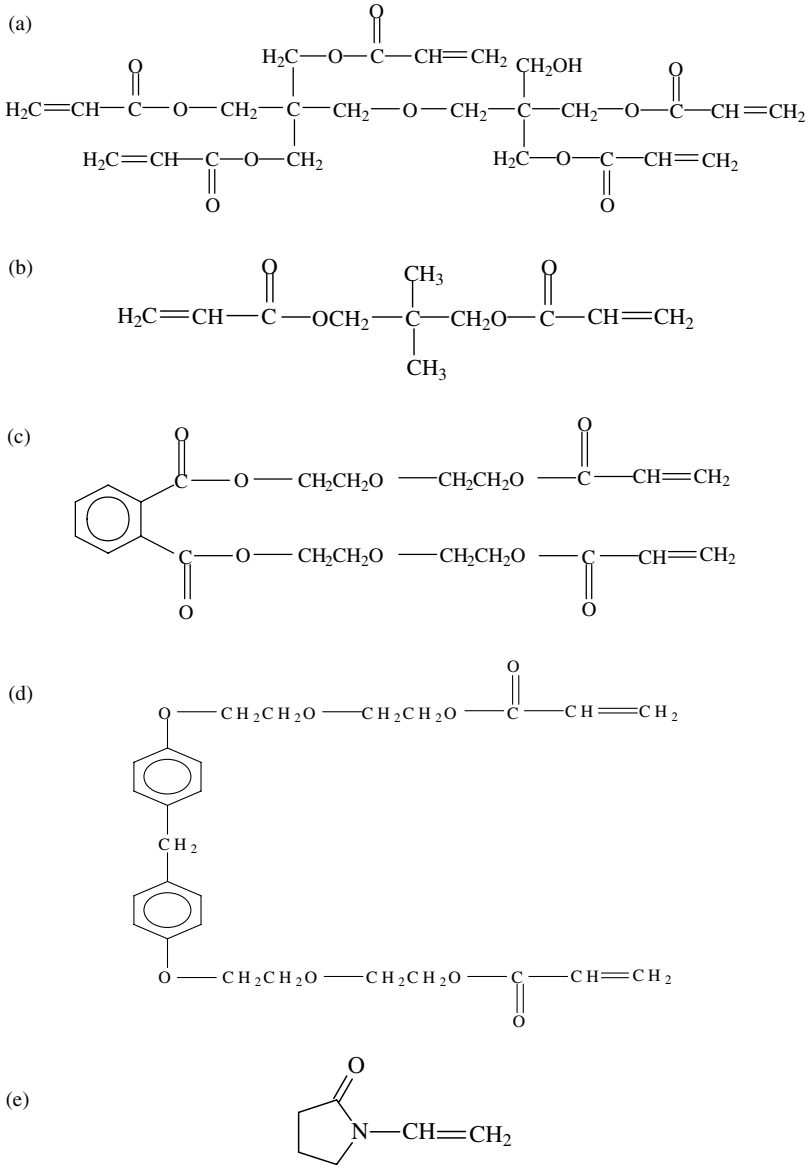

Figure 1. Chemical structure of monomers. DPHPA (*a*), NPGDA (*b*), PDDA (*c*), BPFEDA (*d*), NVP (e).

observation. The samples were immersed in alcohol for about 24 h to extract the remaining LC in the grooves, then fixed on a smooth conductive substrate and blow-dried with high purity nitrogen. All samples were observed by the AFM in the tapping mode. Before the SEM scan, a very thin gold film was always sputter-coated on the surface of the samples as a conductive layer.

The thermo-stability of the polymers formed by mixtures of DN, DP and DB (shown in table 1) were analysed by a thermogravimetric analyzer (PerkinElmer, USA, Pyris Diamond). The mixtures were photopolymerized by the laser, washed with methanol to remove residual impurities, crushed to a powder and then dried with nitrogen flow. The thermogravimetric analyzer was used to monitor weight loss

by heating 4–5 mg of polymer powder from 40 to 750 °C at a rate of 10 °C min^{-1} under a nitrogen purge.

To study the photoreaction kinetics, a FTIR spectrometer (Bio-Red FTS 3000, USA) was employed to detect the carbon–carbon double bond conversion (ene-conversion) during photoreaction. Liquid nitrogen was used to cool the mercury–cadmium–telluride detector and reduce noise from water vapour and carbon dioxide. The H-PDLC grating films were sandwiched between two CaF_2 slices (UP Optotech Co., Ltd., Changchun, China) and fixed on a sample holder. The detection beam was incident normally on the slice. Then, FTIR spectra before and after exposure times of 20 s, 40 s, 60 s, 80 s, 100 s and 15 min were tested with a scan resolution of 2 cm^{-1}. The ene-conversions C after time t could thus be calculated by the absorbance at 1636 cm^{-1},

$$C = \frac{A_t - A_0}{A_0}, \tag{1}$$

where A_0 and A_t represent the absorbance before and after exposure, respectively.

A UV–VIS–NIR spectrometer (Shimadzu UV-3101PC, Japan) was used to analyse the solubility of RB in the mixtures of DN, DP and DB. The mixtures were first filtered to remove any insoluble RB, and diluted with dioxane dioxin (⩾99.8%, from Fluka) to 0.06 mg mL^{-1} before testing. The diluted filtrate was then injected into a quartz vessel of dimensions $1 \times 1 \times 4$ cm^3 for analysis.

3. Experimental results

3.1. Electro-optical characteristics and morphology of H-PDLC gratings at room temperature

The electro-optical properties of three gratings H-PDLC(n), H-PDLC(p) and H-PDLC(b) are shown in figure 2. It can be seen that the diffraction efficiency of H-PDLC(n) is 83%, which is about 10% lower than that of H-PDLC(p) and H-PDLC(b). The tunable range of H-PDLC(p) is the largest among the three while its threshold voltage is the lowest. We also find that the diffraction efficiency of H-PDLC(b) is almost the same as that of H-PDLC(p), but the tunable range of the former is evidently smaller than the latter. This result may be ascribed to the phase separation of LC during photoreaction. As shown in the SEM photographs (figure 3), the LC-rich zone of H-PDLC(p) is broader and the volume of LC droplets is the largest compared with the other two, which are the main reasons for the test results.

3.2. Thermo-stability of the diffraction efficiency

Figure 4 shows the normalized diffraction efficiencies of the three samples after baking at various temperatures. It is evident that the diffraction efficiency of H-PDLC(n) is very unstable, decreasing as the temperature increases. After being baked at 175 °C, its diffraction efficiency drops to only half of the original value at room temperature. On the other hand, the stabilities of H-PDLC(p) and H-PDLC(b) are better, and their diffraction efficiencies remain constant even when the baking temperature rises to 200 °C.

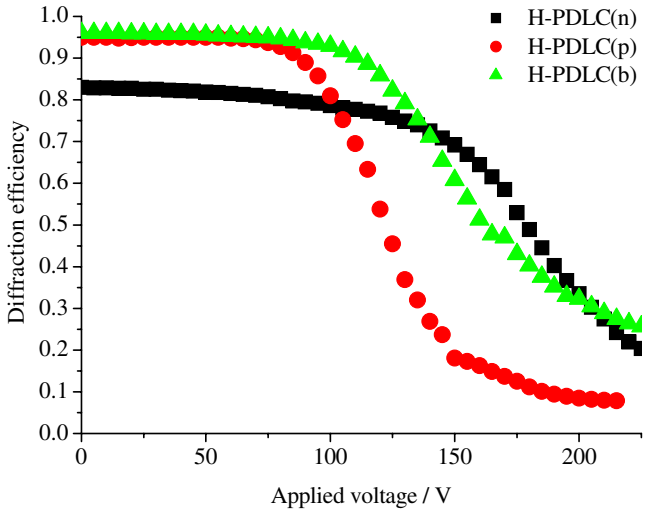

Figure 2. Electro-optical response curve of the H-PDLC gratings (before baking).

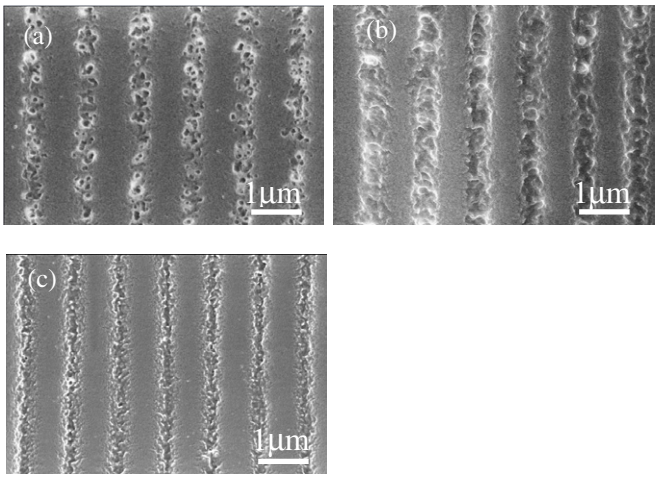

Figure 3. SEM photographs of H-PDLC(n) (*a*), H-PDLC(p) (*b*) and H-PDLC(b) (*c*) before baking.

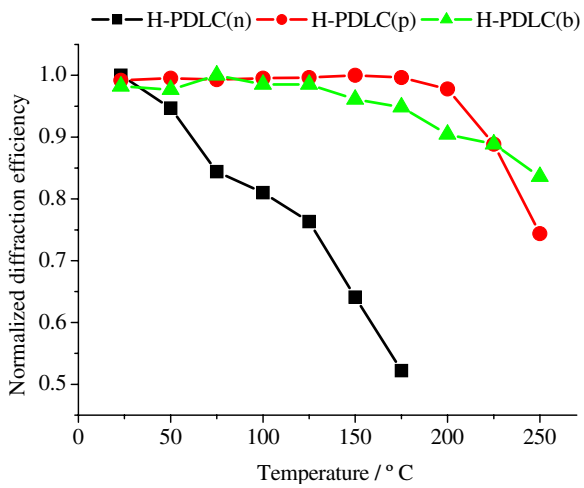

Figure 4. Relationship between normalized diffraction efficiency and the baking temperature.

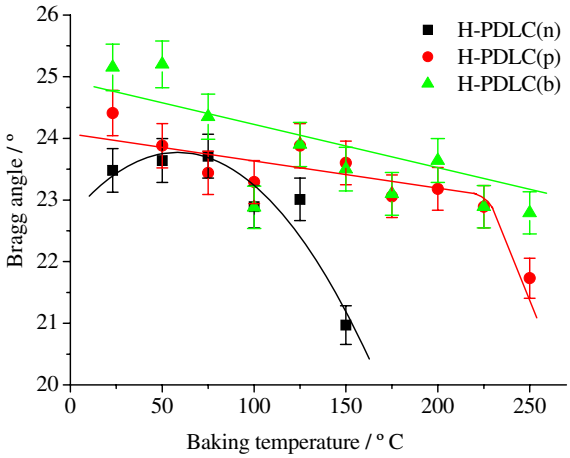

Figure 5. Relationship between Bragg angle and baking temperature. The dots are experimental results; the lines are fitted results.

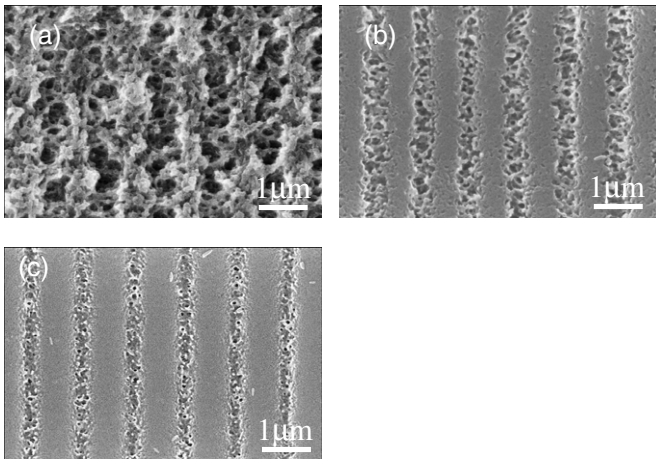

Figure 6. SEM morphologies of H-PDLC(n) (*a*), H-PDLC(p) (*b*) and H-PDLC(b) (*c*) after baking at 250 °C for 10 min.

3.3. Thermo-stability of the Bragg angle

The variation of the Bragg angle with temperature was measured experimentally. As depicted in figure 5, the Bragg angles of all the samples undergo no significant changes until the baking temperature rises over 125 °C. As the temperature continues to increase, the Bragg angle of H-PDLC(n) decreases approximately 2°, but there is no significant change in the other two samples. Figure 5 shows that the Bragg angles of H-PDLC(p) and H-PDLC(b) are very stable when the baking temperature is below 225 °C. The slight fluctuations in the figure, only about 0.3°, may be due to measurement errors. These variations of the Bragg angle are also reflected by the measurements of the diffraction efficiency mentioned in section 3.2.

3.4. Thermo-stability of the morphology

The morphologies of three H-PDLC gratings before and after baking at 250 °C were observed and compared by means of a SEM. Figure 6 shows a fully destroyed structure of H-PDLC(n) at a high temperature, whereas the structures are relatively clear for H-PDLC(p) and H-PDLC(b). To show the microscopic structural changes in the latter two in detail, their periods and groove depths before and after baking were measured by an AFM. As shown in figure 7, the period of H-PDLC(p) changes from 800 nm (figure 7(*a*)) to 917 nm (figure 7(*c*)), while its groove depth decreases from 162 to 110 nm. For H-PDLC(b), the period changes from 800 nm (figure 7(*b*)) to 908 nm (figure 7(*d*)), and its groove depth decreases from 134 to 102 nm. The results agree well with Bragg's law,

$$\frac{d_0}{d_t} = \frac{\sin\theta_B}{\sin\theta_{B0}}, \tag{2}$$

where d_0, d_t and θ_{B0}, θ_B are the periods and Bragg angles of the grating, before and after baking, respectively. As described in section 3.3, for the H-PDLC(p) sample, θ_{B0} and θ_B are approximately 23.5° and 21.5° and d_t and d_0 are 917 nm and 800 nm, respectively, measured by the AFM. Substituting these data into equation (2), we find good agreement between the experimental measurements and Bragg's law. For H-PDLC(b), similar results are obtained.

For the conventional H-PDLC Bragg grating, the thickness of the grating film is much larger than the spacing, that is, the factor $Q \gg 1$ [17]. At normal incidence there is no diffraction beam because Bragg's law is not satisfied. However, if the film thickness is decreased, the diffraction becomes more and more evident under the same conditions, because the value of Q is decreased and the type of grating is Raman–Nath. In our experiments, for a normally incident beam there are two blurred diffractive orders which appear symmetrically distributed on both sides of the transmitted beam. This is caused by the decrease in film thickness, and implies that the H-PDLC has shrunk, as is also proved by the decrease in groove depth. Thus, it can be confirmed that the deformations of H-PDLC(p) and H-PDLC(b) are extensions in the spacing and accompanied by the shrinkage in depth after baking at 250 °C, as illustrated in figure 8.

3.5. Thermo-stability of electro-optical characteristic

Figure 9(*a*) shows that the electro-optical response of H-PDLC(n) disappears completely due to destruction of the structure. Unlike H-PDLC(n), the responses of H-PDLC(p) and H-PDLC(b) (figures 9(*b*) and (*c*)) are almost the same as their original performance (squares).

These experimental results indicate that the structure and electro-optical response of H-PDLC(p) and H-PDLC(b) are very good even after they are baked at a high temperature. Although we find that structure variation appears after baking at 225 °C, its effect on electro-optical switchability is very small. However, the diffraction efficiency (figure 4), structure (figure 6(*a*)) and response (figure 9(*a*)) of H-PDLC(n) are very unstable at a much lower baking temperature compared with the above two samples.

4. Discussions

Some of the factors that influence the thermo-stability of H-PDLC gratings will now be discussed.

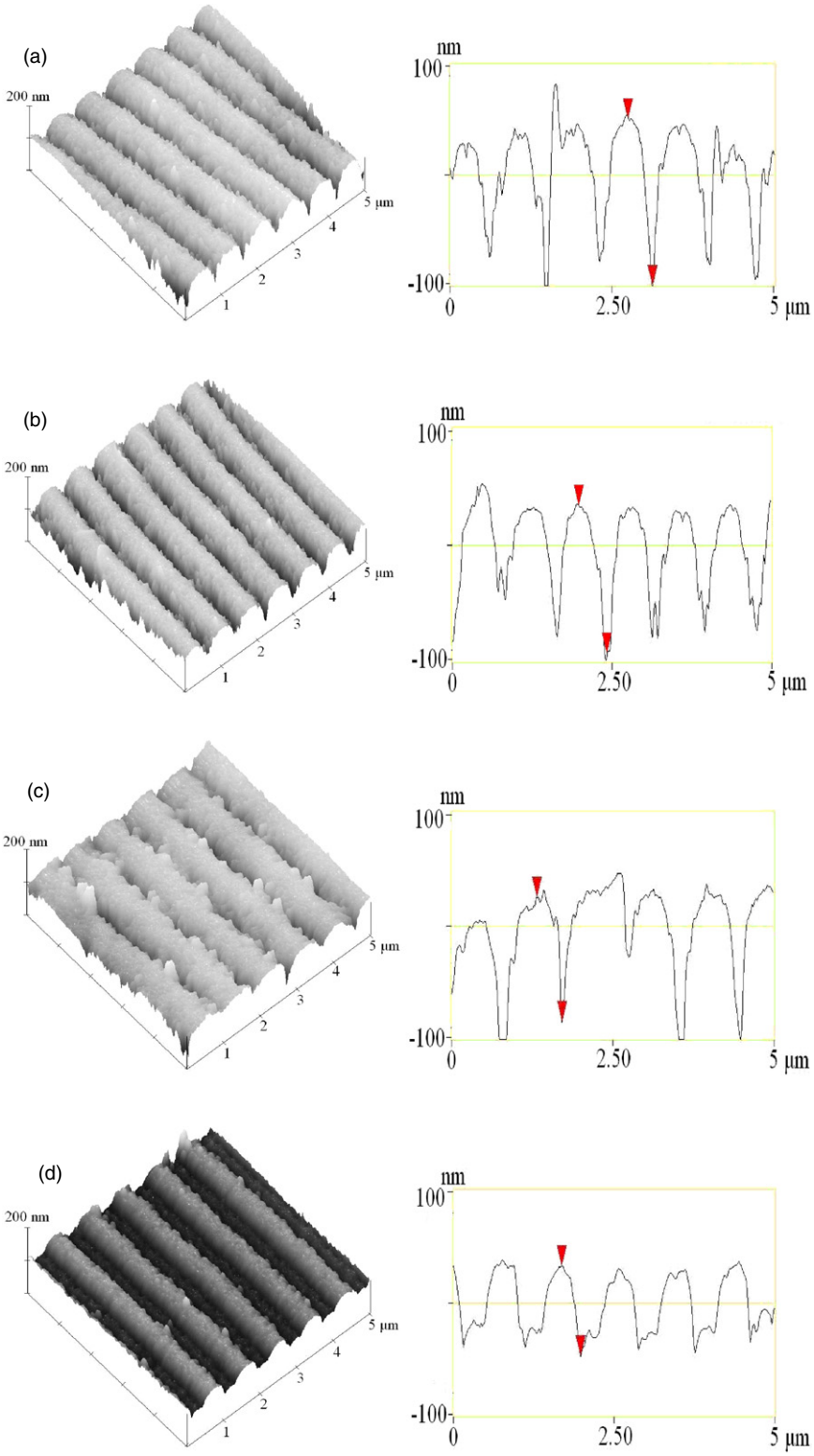

Figure 7. AFM morphology and corresponding side-view analysis of H-PDLC(p) without baking (*a*) and after baking at 250 °C (*c*); Similarly for H-PDLC(b) without baking (*b*) and after baking at 250 °C (*d*).

4.1. Chemical structure

The chemical structure of the material has a direct influence on the thermo-stability. To elucidate this, the thermogravimetry losses of polymers P_{DN}, P_{DP} and P_{DB} formed by monomer mixtures DN, DP and DB (shown in table 1) were measured by means of the thermogravimetric analyzer, and the results are displayed in figure 10. It is shown that the decomposition temperature (T_d) of P_{DN} is about 198 °C, which is 80 ∼ 100 °C lower than the T_d values of 283 °C and 302 °C for P_{DP} and P_{DB}, respectively. The latter are higher due to the rigidity ring in the P_{DP} and P_{DB} monomer structures (see figures 1(*c*)

and (*d*)), which significantly increases the interactions and restricts the motion between the molecules. Moreover, the bond energy of such rigidity rings is higher than that of flexible chain structures. Therefore, the higher T_d of P_{DP} and P_{DB} are reasonable.

Furthermore, the decomposition activation energies of the above polymers have been calculated by the Freeman–Carroll differential method [44], which can be expressed by the following equation

$$\frac{\Delta \lg\left(-\frac{1}{m_0-m_\infty}\cdot\frac{dm}{dt}\right)}{\Delta \lg\left(\frac{m-m_\infty}{m_0-m_\infty}\right)} = \frac{-E}{2.303R}\cdot\frac{\Delta\left(\frac{1}{T}\right)}{\Delta \lg\left(\frac{m-m_\infty}{m_0-m_\infty}\right)} + n. \quad (3)$$

Here m_0 and m_∞ are the sample weights at the beginning and end of the measurements, respectively; dm/dt on the left-hand side represents the instantaneous decomposition rate of the sample, and can be obtained directly from the differential thermogravimetry (DTG) curve. As usual, R and T on the right-hand side are the molar gas constant and Kelvin temperature, E and n denote the decomposition activation energy and the corresponding reaction order, respectively, while Δ is the difference operator.

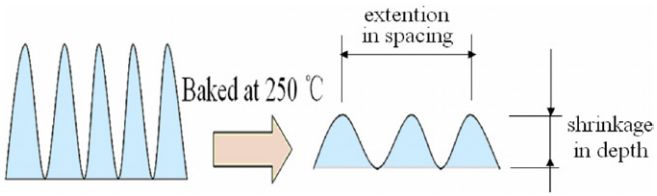

Figure 8. Schematic of the deformation of the H-PDLC.

We define the independent variable in equation (3) as

$$X = \frac{1}{2.303R}\cdot\frac{\Delta\left(\frac{1}{T}\right)}{\Delta \lg\left(\frac{m-m_\infty}{m_0-m_\infty}\right)}$$

and the dependent variable as

$$Y = \frac{\Delta \lg\left(-\frac{1}{m_0-m_\infty}\cdot\frac{dm}{dt}\right)}{\Delta \lg\left(\frac{m-m_\infty}{m_0-m_\infty}\right)},$$

thus equation (3) can be expressed as a linear equation in the form $Y = -E \times X + n$. In this way, the decomposition activation energy E and reaction order n can be calculated by the slope and y-intercept of the line.

The calculated decomposition activation energies and their corresponding reaction orders for three samples (labelled P_{DN}, P_{DP} and P_{DB}, see abbreviation section) are shown in the right-hand column of figure 10. For sample P_{DN}, the fitted linear equation is $Y = -7.39 \times 10^4 X + 1.217$, so the slope and the y-intercept are -7.39×10^4 and 1.217, respectively, the activation energy is $E_{DN} = 73.9\,\mathrm{kJ\,mol^{-1}}$, and the reaction order is $n_{DN} = 1.217$. Similarly, for P_{DP} we obtain $E_{DP} = 142.5\,\mathrm{kJ\,mol^{-1}}$ and $n_{DP} = 2.802$ and for P_{DB}, $E_{DB} = 151.6\,\mathrm{kJ\,mol^{-1}}$ and $n_{DB} = 4.770$. The calculated results show that sample P_{DN} has the lowest activation energy and exhibits the greatest instability compared with P_{DP} and P_{DB}. The activation energy of P_{DB} is a little higher than P_{DP} (less than $10\,\mathrm{kJ\,mol^{-1}}$), which indicates that they have similar thermo-stability. The reaction order can be used to reflect the ease or difficulty of a reaction. The smaller the order, the easier the reaction. The relationship among the reaction orders, $n_{DN} < n_{DP} < n_{DB}$, shows that the thermo-decomposition occurs easily in sample P_{DN} but less so in

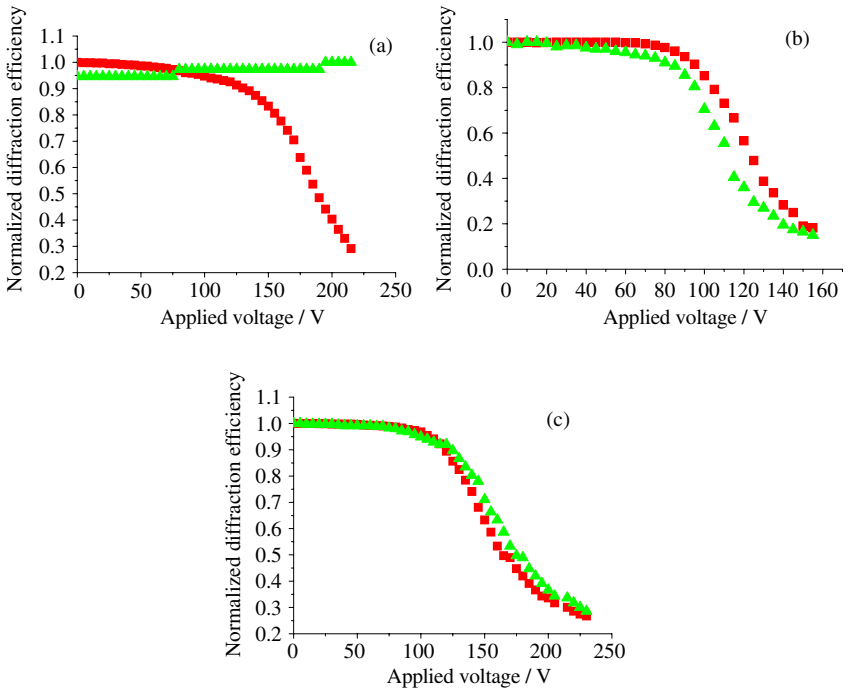

Figure 9. Electro-optical response of H-PDLC(n) (*a*), H-PDLC(p) (*b*) and H-PDLC(b) (*c*), the normalized diffraction efficiency versus applied voltage. Squares, before baking; triangles, after baking at 175 °C (for figure (*a*)) and 250 °C (for figures (*b*) and (*c*)).

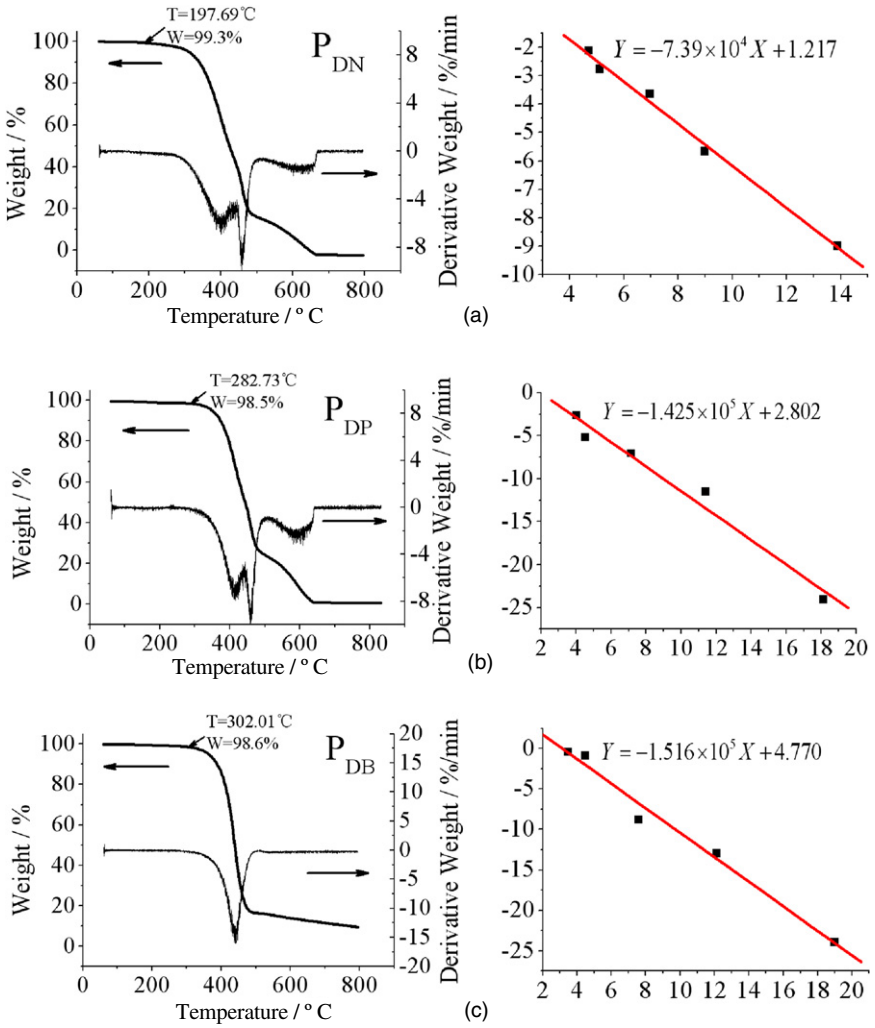

Figure 10. Thermogravimetry analysis of polymers P_{DN} (*a*), P_{DP} (*b*) and P_{DB} (*c*). The left column shows the TG and corresponding DTG curves. The right column shows analytical lines for the decomposition activation energy calculated by the Freeman–Carroll methods. In the right column the *x*-axes in the figures are $\frac{1}{2.303R}\frac{\Delta(T^{-1})}{\Delta\lg\left(\frac{m-m_\infty}{m_0-m_\infty}\right)} \times 10^{-5}$, the *y*-axes are $\frac{\Delta\lg\left(-\frac{1}{m_0-m_\infty}\cdot\frac{dm}{dt}\right)}{\Delta\lg\left(\frac{m-m_\infty}{m_0-m_\infty}\right)}$ and the square dots denote the calculated results from the TG and DTG curves. The fitted lines and functions of the lines are also shown.

P_{DP} and P_{DB}. In addition, P_{DB} has the largest reaction order, which suggests that its decomposition is most difficult. These TG analysis results imply that the thermo-stability of a polymer is very closely related to its chemical structure. A rigid structure can lead to substantial improvement of the thermo-stability.

In addition, we have characterized the LC stability by testing the LC alignment behaviour at different baking temperatures. An anti-parallel cell is assembled, the cell gap is 12 μm and the alignment film is polymide SE-410 (from Nissan Chemical Industries, Ltd.), which has very good thermo-stability at 250 °C [45] so it is unnecessary to consider its effect on the LC alignment at high temperatures. The LC TEB30A was injected into the cell and baked under the same temperature conditions mentioned in section 2.2, then cooled to room temperature. The LC alignment behaviour is usually evaluated by contrast ratio measurements with a polarized optical microscope (Olympus BX-51). Figure 11 gives the contrast ratio of the cell after baking. It seems that the ratio stabilizes to a value of 220 when the temperature is lower than 200 °C. However, after the cell is baked at 250 °C, the ratio drops drastically to 60, which indicates that disordering of the LC alignment has occurred due to thermal effects, such as melting or decomposition.

Recalling the thermo-stability test results given in section 3, we see that the instability of the grating H-PDLC(n) lies mainly in the poor stability of polymer P_{DN}, because the polymer chains move easily at high temperature, which leads to deformation of the structure (figure 6(*a*)) and, subsequently, to the decrease in diffraction efficiency (figure 4) and changes in the Bragg angle (figure 5). However, for the H-PDLC(p) and H-PDLC(b) samples, because the ring rigidity in the polymer molecules increases the molecular interactions and restricts the polymer chain movements, their polymer stability is better than that of H-PDLC(n). Consequently, we find good thermo-stability of their structure and optical and switch characteristics. Another point which should be mentioned is that thermal destructions of the LC at high baking temperatures may probably be avoided by the protection of the polymer network which encapsulates the LC droplet. Thus the

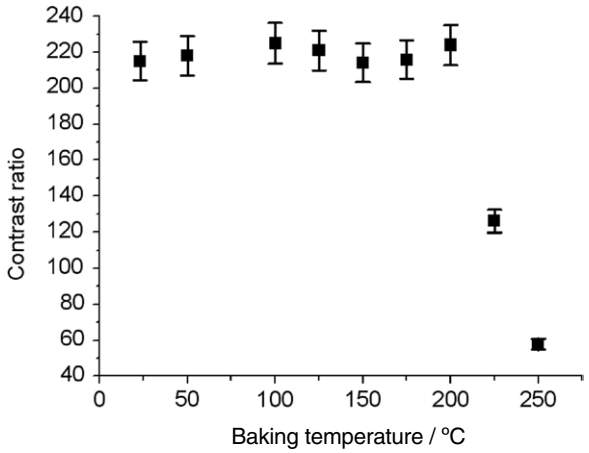

Figure 11. Contrast ratio of TEB30A at different baking temperatures.

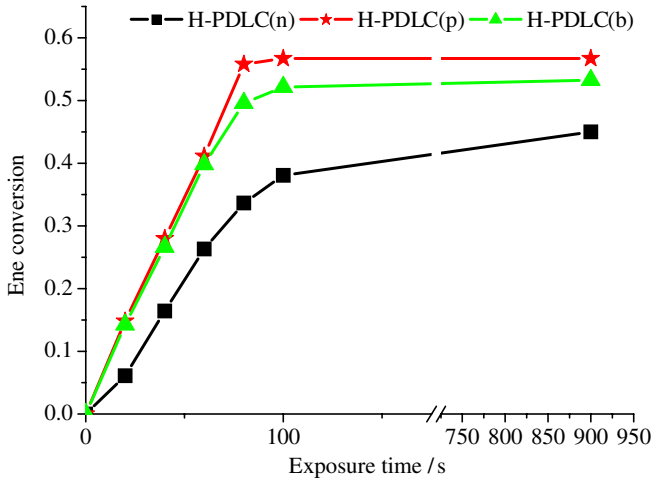

Figure 12. Ene-conversions of the H-PDLCs during exposure.

switchability of H-PDLC(p) and H-PDLC(b) is still good after they are baked at 250 °C despite the fact that pure LC can only withstand 200 °C baking.

4.2. Photoreaction kinetics

From the photoreaction kinetics point of view, certain other influences on the thermo-stability should also be considered. The ene-conversions (defined in section 2.2 and calculated by equation (1)) of the three samples have been measured and are shown in figure 12, where we find that H-PDLC(n) has the lowest value, about 0.45 for an exposure time of 15 min. In contrast, the values are 0.58 and 0.53, respectively, for H-PDLC(p) and H-PDLC(b), which are approximately 0.1 higher than for H-PDLC(n). Moreover, the figure clearly shows that the ene-conversions of H-PDLC(p) and H-PDLC(b) reach saturation after 100 s, but not with H-PDLC(n). That is to say, the photoreaction rate of H-PDLC(n) is significantly lower than that of the other two. The reason for this lies in the difference of photoreaction efficiency in the systems.

We note that the photoinitiative system, average functionality of the monomers and exposure intensity and wavelength were all the same in our experiments, so it could

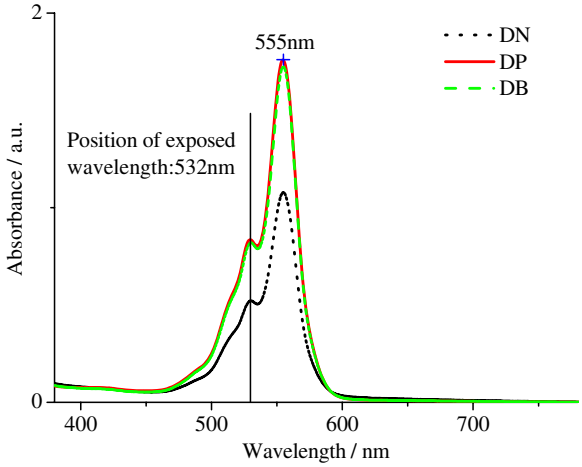

Figure 13. Absorbance versus wavelength spectra of the monomer mixtures. The peak at 555 nm reflects the absorbance of RB.

be supposed that the most possible reason for the different reaction efficiencies lies in the solubility of the photoinitiator in the monomer mixtures. To prove this, the visible absorbance spectra of the photoinitiator (RB in our experiments) in the mixtures were measured and plotted in figure 13. The solubility of RB in the mixture can be reflected by the total peak area of the spectrum, and it is clear that the DN system has the smallest area compared with the other two; however, the areas of the DP and DB mixtures are almost the same. Consequently, we believe that the solubility of RB is not very good in the DN mixture. In addition, the absorbance of DN at 532 nm is lower than in the other samples, and the FTIR spectra also show that the polymerization rate is the slowest and the ene-conversion is the lowest, which indicate a lower photoreaction efficiency in this DN system. Another point is that there is a small discrepancy between DP and DB ene-conversions, the value of the latter being 0.05 lower than the former. This reason may account for the immobility and steric hindrance of the more rigid molecular structure in DB, which influences the consumption and crosslinking of the double bond.

We may consider the influence of the photoreaction kinetics on the grating thermo-stability from two aspects. On the one hand, according to the basic principle of free-radical polymerization, the propagation rate R_P is proportional to the square-root of the concentrations of the photoinitiator Φ_R, as shown in the equation below [46],

$$R_P = k_P[M]\left(\frac{\varepsilon f_i I_0 \phi_R l}{k_t}\right)^{1/2}. \quad (4)$$

Here $[M]$ is the monomer concentration; k_p and k_t are the propagation rate and termination rate constants, ε and f_i the molar extinction coefficient and quantum yield of photoinitiator and I_0 and l the exposure intensity and sample thickness, respectively. The lower photoinitiator solubility results in a lower concentration in the mixture, and subsequently decreases the propagation rate of the polymer chain and leads to the formation of oligomers which are very unstable at high temperature. The crosslinking density in such a system is also lower, so the polymer network easily deforms at a high temperature.

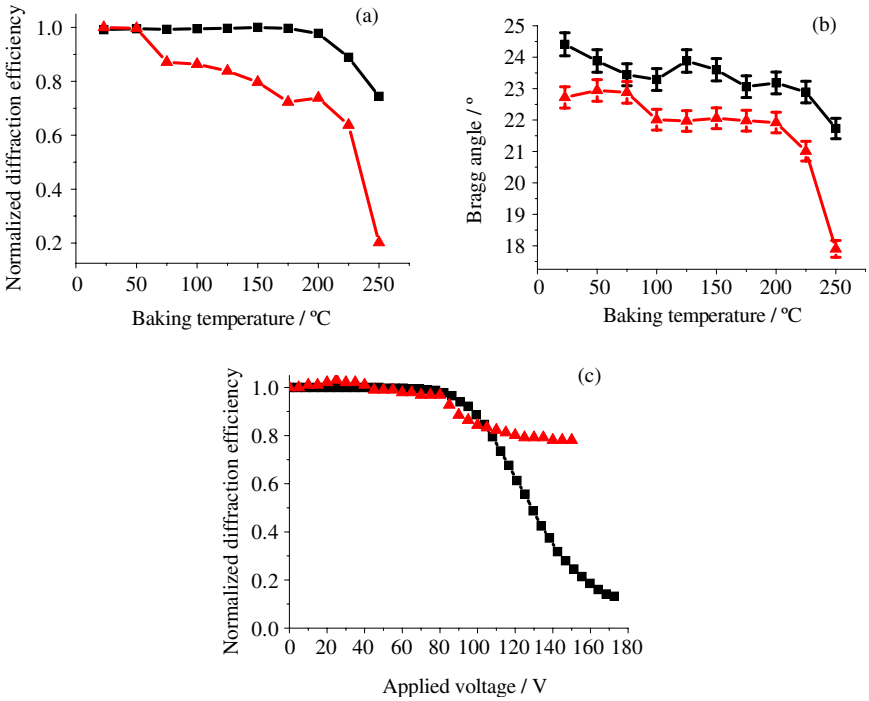

Figure 14. Thermo-stabilities of H-PDLC(p) and H-PDLC(2.88). Diffraction efficiency (*a*) and Bragg angle (*b*) versus the baking temperature and electro-optical tenability characteristic of H-PDLC(2.88) (*c*). In figures (*a*) and (*b*), squares represent H-PDLC(p), triangles represent H-PDLC(2.88). In figure (*c*), squares denote before baking and triangles after baking at 250 °C.

During PIPS, monomers are consumed and form polymers. Simultaneously, LCs are squeezed out of the polymer network, and diffuse into the reaction system. This will lead to a change in chemical potential, which is usually expressed as [47–49]

$$\mu_\beta = \mu_{\beta 0} + kT \ln\left(\frac{N_\beta}{\sum_i N_i}\right), \tag{5}$$

where $\mu_{\beta 0}$ is the chemical potential of the pure β component, N_β the number of β molecules, i the number of components in the system, k Boltzmann's constant and T the Kelvin temperature. During exposure, more monomers are consumed in the high interference intensity zone compared with the low intensity zone, and thus the chemical potential of the monomers in the former is decreased, according to equation (5). However, the LC chemical potential is increased due to the consumption of monomers (because ΣN_i decreases while N_{LC} does not change) [13, 14]. To reach thermodynamic equilibrium, the monomers diffuse from a low intensity zone (high chemical potential) to a high one (low chemical potential); conversely, the LCs counter-diffuse from the high to the low zone. The chemical potential gradient causes molecular diffusion between high and low intensity zones, which is a promotion source for the phase separation. In the case of low photoreaction efficiency system (such as DN), this gradient is very small; consequently, the diffusion of monomers and LCs is limited and the crosslinking density is also lower. In addition, because of this low efficiency, there may be a lot of residual monomers in the grating, which would move into the polymer network, thermo-polymerize (normally at 100 °C [50, 51]), and destroy the original structure of the grating, thus influencing its thermo-stability.

Hence, a low efficiency photoreaction system is detrimental to the thermo-stability of the H-PDLC grating. To improve this, the solubility of the photoinitiator in the mixture needs to be considered. At the same time, some high efficient photoinitiator can be tried.

4.3. Average functionality (f) of monomers

A mixture of $f = 2.88$ was used to fabricate an H-PDLC grating (labelled H-PDLC(2.88)), which was compared with H-PDLC(p) formed from a similar mixture of $f = 3.39$. In this experiment, NVP was used to modulate the average functionality. Some previous researchers have reported that adding NVP to the materials can increase crosslinking density and enhance ene-conversion [17, 52]. However, according to White's report [53], these effects can be ignored when the content of NVP is rather low (only 4 wt% in the experiment).

The thermo-stabilities of H-PDLC(p) and H-PDLC(2.88)) have also been investigated through their diffraction efficiency, Bragg angle and electro-optical response. As shown in figure 14, the diffraction efficiency of H-PDLC(2.88) starts to change at 75 °C, which is much lower than the 225 °C of H-PDLC(p). The Bragg angle drops drastically from 22° to 17.5° for H-PDLC(2.88), but it is almost constant for the high functionality sample, H-PDLC(p), even though the temperature reaches 225 °C. The drop in diffraction efficiency may be closely related to the change in the grating structure and the decrease in Bragg angle. The electro-optical response of the low functionality sample H-PDLC(2.88) exhibits a worse thermo-stability performance.

We believe that the main reason for the bad thermo-stability of H-PDLC(2.88) may be ascribed to the incomplete phase separation. As reported by Park and Kim [54] and Pogue *et al* [55], the polymerization rate seems slow in a low functionality system (the number of double bonds in the material is small), so the crosslinking density is lower and the polymer network is looser, which is insufficient to squeeze more LCs out of it. As a result, the polymer thermo-stability is decreased due to more LCs entrapped in its network. From another aspect, the low functionality of the monomers leads to a loose polymer network which would deform easily at high baking temperatures, thus the thermo-stability of the grating is bad. Hence it seems that low functionality of monomers not only influences phase separation, but also decreases thermo-stability. These shortcomings can be improved by adding some efficient additives, such as fluorine-substituted acrylate monomer [56]. Other related studies are being carried out in our group.

5. Conclusions

The thermo-stability of acrylate based H-PDLC gratings have been evaluated from their diffraction efficiency, Bragg angle, electro-optical response and morphology. Some major aspects of the thermo-stability have been analysed and discussed, from which we may draw the following conclusions.

(a) The chemical structure of the monomers plays an important role in the thermo-stability performance of H-PDLC gratings. A rigid molecular structure forms a hard polymer network which is very stable at high temperatures. In addition, the ring rigidity increases interactions between molecules and restricts the motion between them, thus enhancing the thermo-stability.

(b) An efficient photoreaction system increases the crosslinking density of polymer and promotes the phase separation between the LC and polymer, which helps to improve the thermo-stability of the grating structure. The solubility of the photoinitiator in the mixture is an important factor which needs to be considered. Our experiments indicate that a good solubility leads to high reaction efficiency.

(c) A lower average functionality is detrimental to the thermo-stability of the grating due to incomplete phase separation and a loose polymer network. Incorporating some additives to promote phase separation and increase the polymer hardness may be a feasible means of improvement.

Acknowledgments

This work was supported by the National Natural Science Foundation of China (Grant Nos 60578035 and 50703039); the State Key Foundation (Grant No 60736042) and the Science Foundation of Jilin Province (Grant Nos 20050520 and 20050321-2). The authors would also like to thank Mr Shu Pei and Dr Haifeng Zhao for their kind help with the AFM and SEM.

References

[1] Ren H and Wu S T 2003 *Appl. Phys. Lett.* **82** 22
[2] Fan Y H, Ren H and Wu S T 2003 *Opt. Express* **11** 3080
[3] Liu Y J and Sun X W 2006 *Appl. Phys. Lett.* **89** 171101
[4] Liu Y J, Sun X W, Shum P and Yin X J 2006 *Opt. Express* **14** 5634
[5] Wu S T and Fuh A Y 2004 *Japan. J. Appl. Phys.* **43** 7077
[6] Wu S T and Fuh A Y 2006 *Japan. J. Appl. Phys.* **45** 7011
[7] Liu Y J, Sun X W, Liu J H, Dai H T and Xu K S 2005 *Appl. Phys. Lett.* **86** 041115
[8] Bowley C C, Fontecchio A K, Crawford G P, Lin J J, Li L and Faris S 2000 *Appl. Phys. Lett.* **76** 523
[9] Massenot S, Kaiser J L, Perez M C, Chevallier R and Tocnaye J L 2005 *Appl. Opt.* **44** 5273
[10] Gorkhali S P, Qi J and Crawford G P 2005 *Appl. Phys. Lett.* **86** 011110
[11] Zheng Z, Song J, Liu Y, Guo F, Ma J and Xuan L 2008 *Liq. Cryst.* **35** 489
[12] Sun X, Tao X, Ye T, Xue P and Szeto Y S 2007 *Appl. Phys.* B **87** 267
[13] Bunning T J, Natarajan L V, Tondiglia V P, Dougherty G and Sutherland R L 1997 *J. Polym. Sci.* B **35** 2825
[14] Bunning T J, Natarajan L V, Tondiglia V P, Sutherland R L, Veziet D L and Adams W W 1995 *Polymer* **36** 2699
[15] Lee J C 1999 *Phys. Rev.* E **60** 1930
[16] Buil S, Hugonnot E and Delville J P 2001 *Phys. Rev.* E **63** 041504
[17] Bunning T J, Natarajan L V, Tondglia V P and Sutherland R L 2000 *Annu. Rev. Mater. Sci.* **30** 83
[18] Sutherland R L, Natarajan L V, Tondiglia V P, Bunning T J and Adams W W 1994 *Appl. Phys. Lett.* **64** 1074
[19] Shih H F and Tsai C Y 2005 *Japan. J. Appl. Phys.* **44** 7491
[20] Tanaka K, Kato K and Date M 1999 *Japan J. Appl. Phys.* **38** L277
[21] Schulte M D, Clarson S J, Natarajan L V, Tomlin D W and Bunning T J 2000 *Liq. Cryst.* **27** 467
[22] Sarkar M D, Qi J and Crawford G P 2002 *Polymer* **43** 7335
[23] Veltri A, Caputo R, Umeton C and Sukhov A V 2004 *Appl. Phys. Lett.* **84** 3492
[24] Caputo R, Sio L D, Veltri A, Umeton C and Sukhov A V 2004 *Opt. Lett.* **29** 1261
[25] Jazbinsek M, Olenik I D, Zgonik M, Fontecchio A K and Crawford G P 2001 *J. Appl. Phys.* **90** 3831
[26] Colvin V L, Larson R G, Harris A L and Schilling M L 1997 *J. Appl. Phys.* **81** 5913
[27] Vardanyan K K, Qi J, Eakin J N, Sarkar M D and Crawford G P 2002 *Appl. Phys. Lett.* **81** 4736
[28] Sutherland R L, Tondiglia V P, Natarajan L V and Bunning T J 2004 *J. Appl. Phys.* **96** 951
[29] Sutherland R L, Tondiglia V P, Natarajan L V, Lloyd P F and Bunning T J 2006 *J. Appl. Phys.* **99** 123104
[30] Sutherland R L 2002 *J. Opt. Soc. Am.* B **19** 2995
[31] Scherschener E, Perciante C D, Dalchiele E A, Frins E M, Kom M and Ferrari J A 2006 *Appl. Opt.* **45** 3482
[32] Fox A E, Rai K and Fontecchio A K 2007 *Appl. Opt.* **46** 6277
[33] Chanclou P, Vinouze B, Roy M, Cornu C and Ramanitra H 2003 *J. Light. Technol.* **21** 3471
[34] Dick V P and Loiko V A 2004 *J. Phys. D: Appl. Phys.* **37** 1834
[35] Jakubiak R, Bunning T J, Vaia R A, Natarajan L V and Tondiglia V P 2003 *Adv. Mater.* **15** 241
[36] Date M, Takeuchi Y and Kato K 1998 *J. Phys. D: Appl. Phys.* **31** 2225
[37] Sanchez C, Escuti M J, Heesch C, Bastiaansen C W M and Broer D J 2005 *Appl. Phys. Lett.* **87** 094101
[38] Murai H and Gotoh T 1993 *Mol. Cryst. Liq. Cryst.* **226** 13
[39] Snively C, Chen P Y, Palmer R A and Koenig J L 1996 *Mol. Cryst. Liq. Cryst.* **289** 11

[40] Im S J, Park K S, Noh C H, Jung J E, Lee S J and Sakong D S 1997 *Mol. Cryst. Liq. Cryst.* **295** 109
[41] Cairns D R, Bowley C C, Danworaphong S, Fontecchio A K, Crawford G P, Li L and Faris S M 2000 *Appl. Phys. Lett.* **77** 2677
[42] Qi J, Sarkar M D, Warren G T and Crawford G P 2002 *J. Appl. Phys.* **91** 4795
[43] Park M S, Kim B K and Kim J C 2003 *Polymer* **44** 1595
[44] Segal E and Fatu D 1976 *J. Therm. Anal.* **9** 65
[45] According to product instruction supplied by Nissan Chemical Industries, Ltd.
[46] Odian G 2004 *Principles of Polymerization* (Hoboken, NJ: Wiley)
[47] Shen C and Kyu T 1994 *J. Chem. Phys.* **102** 556
[48] Chiu H W and Kyu T 1995 *J. Chem. Phys.* **103** 7471
[49] Kyu T and Chiu H W 1996 *Phys. Rev.* E **53** 3618
[50] Zhong Z Z, Schuele D E, Gordon W L, Adamic K J and Akins R B 1992 *J. Polym. Sci.* B **30** 1443
[51] Mucha M and Krolikowski Z 2002 *Proc. SPIE* **4759** 473
[52] Bunning T J, Natarajan L V, Tondiglia V P and Sutherland R L 1996 *Proc. SPIE* **2651** 44
[53] White T J, Liechty W B, Natarajan L V, Tondiglia V P, Bunning T J and Guymon C A 2006 *Polymer* **47** 2289
[54] Park M S and Kim B K 2006 *Nanotechnology* **17** 2012
[55] Pogue R T, Natarajan L V, Siwecki S A, Tondiglia V P, Sutherland R L and Bunning T J 2000 *Polymer* **41** 733
[56] Zheng Z, Ma J, Li W, Song J, Liu Y and Xuan L 2008 *Liq. Cryst.* **35** 885